Tellus (2003), 55B, 993–1006
Printed in UK. All rights reserved

TELLUS

Analysis of the Algerian severe weather event in November 2001 and its impact on ozone and nitrogen dioxide distributions

By W. THOMAS[1]*, F. BAIER[2], T. ERBERTSEDER[2] and M. KÄSTNER[2], [1]*Institut für Methodik der Fernerkundung (IMF), and* [2]*Deutsches Fernerkundungsdatenzentrum (DFD), Deutsches Zentrum für Luft- und Raumfahrt (DLR), P.O. Box 1116, D-82234 Wessling, Germany*

(Manuscript received 1 July 2002; in final form 14 April 2003)

ABSTRACT

An analysis of the severe weather event in November 2001 over the western Mediterranean is presented focusing on satellite-based trace gas measurements from the Global Ozone Monitoring Experiment (GOME) on board the European Remote Sensing Satellite (ERS-2). This study is supplemented by a synoptic analysis and simulations of the three-dimensional stratospheric chemical transport model ROSE. Arctic air masses moved rapidly from Scandinavia to the Iberian peninsula and were mixed with subtropical air over the still warm Mediterranean Sea. This caused severe thunderstorms and extreme rainfall along the coasts of Morocco and Algeria and later on the Balearic Islands. Associated with the meridional transport an intrusion of stratospheric air below 3 km above sea level was observed. The maximum potential vorticity (PV) derived from UK Meteorological Office analysis data was about 9.3 potential vorticity units (pvu) at 330 K at the equatorward position of 35°N. These very high values went along with remarkably enhanced total ozone levels obtained from GOME backscatter measurements of collocated GOME/ERS-2 overpasses. Further investigation of GOME data showed unusually high levels of nitrogen dioxide (NO_2) above the western Mediterranean. We present a new method to derive the tropospheric content of nitrogen dioxide (NO_2) from a combination of satellite measurements and results of a chemical transport model. We show that about two-third of the total atmospheric content of nitrogen dioxide in the observed plume is found in the troposphere, due to lightning activity, advection and vertical transport in the thunderstorms from the planetary boundary layer (PBL) to atmospheric levels above clouds.

1. Introduction

From 9 to 11 November 2001, a series of heavy thunderstorms was observed over Morocco, Algeria and the Balearic Islands that caused severe damage to the infrastructure, mainly due to flooding. Although heavy rain and cyclones are typical events in the western Mediterranean in winter, more than 750 people died in the flood ("el hemla"), which was the second worst natural disaster in Algeria during the last 40 years. The unusual pattern of the spatial distribution of total ozone and nitrogen dioxide during this weather event, both derived from GOME nadir backscatter measurements, drew our attention to it and we analysed its temporal and spatial evolution in the stratosphere and the troposphere. We further used the three-dimensional (3D) chemical-dynamical transport model ROSE (Rose and Brasseur, 1989) to simulate transport and the nitrogen dioxide background distribution in the stratosphere and to compare the latter with GOME measurements. A new method was developed that combines satellite observations and ROSE results in order to derive the tropospheric nitrogen dioxide content.

This severe weather event originated from an arctic cold front along which air masses moved

*Corresponding author.
e-mail: werner.thomas@dlr.de

within two days over several thousand kilometres southward from Scandinavia over the Iberian peninsula to North Africa, where cyclogenesis started. Cyclogenesis is a well known process for cut-off lows when air masses of relatively high potential vorticity (PV) rapidly push down southwards from polar regions. Approaching the axis of the trough in a Rossby wave a conversion of static stability into absolute vorticity takes place by stretching of the vertical air column. The formation of a cut-off low starts and coincides in this case with the dry intrusion of stratospheric air, which occurs frequently (Kentarchos et al., 1998). These processes are triggered by PV anomalies, as recently described by Bluestein (1993). Due to the large-scale Rossby wave pattern ozone-rich air in the lower stratosphere is transported southward.

Nitrogen oxides play a key role in the formation of tropospheric ozone, a photochemical process that remarkably influences the chemical composition of the atmosphere. The quantitative contributions of both natural and anthropogenic tropospheric sources of nitrogen dioxide to the total NO_2 budget are not very well known, due to sparse ground-based measurements. Here, satellite-based measurements may contribute significantly to provide tropospheric nitrogen dioxide levels on a global scale (Lauer et al., 2002; Velders et al., 2001; Martin et al., 2002). Recent airborne measurements substantiated the supposition that considerable contributions originate from lightning in thunderstorms and vertical transport of polluted air masses (i.e. NO_2-rich air) from the planetary boundary layer (PBL) to higher atmospheric levels (Huntrieser et al., 2002; Brunner et al., 2001). At the tropopause level further contributions from air traffic have also to be taken into account (Schumann, 1994). In the upper stratosphere NO_2 is mainly produced via atomic oxygen from nitrous oxide (N_2O) and is subsequently transported poleward into the lower stratosphere. There, denitrification and transport into the troposphere contribute to the main loss processes. The daily averaged stratospheric NO_2 column is dominated by available solar insolation and shows a pronounced latitudinal dependency, while tropospheric NO_2 levels are highly variable in time and space.

The trace gas retrieval technique and the ROSE model are described in section 2; in section 3 we present the synoptic analysis of the troposphere and stratosphere, the 3D results of ROSE, and the derivation of the tropospheric nitrogen dioxide content. Our conclusion is given in section 4.

2. Data

2.1. Trace gas measurements

The impact of a severe weather event on the chemical composition of the atmosphere is analysed using backscatter measurements from the Global Ozone Monitoring Experiment (GOME) on board the ERS-2 satellite (see e.g. Burrows et al., 1999 and references therein). An enhanced version of the operational GOME Data Processor (GDP) as described in Loyola et al. (1997) was used to derive total column results of ozone and nitrogen dioxide. The GOME spectrometer is able to measure the atmospheric columnar content of a number of minor trace constituents (e.g. ozone, nitrogen dioxide, bromine monoxide, sulfur dioxide, formaldehyde, chlorine dioxide) between 240 and 793 nm, with spectral resolutions varying from 0.2 to 0.4 nm. GOME is a nadir-looking across-track scanning instrument with a typical footprint size of about 320×40 km^2.

Since GOME pixels cover a relatively large area, the footprints will often be partially or totally covered by clouds. Clouds are opaque in the UV/VIS spectral range (except optically thin cirrus clouds), which need to be taken into account if trace gas total columns are retrieved. The cloud coverage of a GOME footprint is determined by a linear least-squares fit of GOME spectra to simulated spectra in and around the oxygen A-band between 758 and 778 nm. We use a relationship between the measured absorption depth in the oxygen A-band, the cloud optical thickness, the cloud-top height and the fractional cloud cover of a GOME pixel as described in detail by Kuze and Chance (1994). Cloud coverage results from GOME can be lower than corresponding results from other satellite sensors (Koelemeijer and Stammes, 1999) but compare reasonably well if optically thick clouds are present, as it is mainly the case in our study (see e.g. Fig. 2).

The core element of the retrieval package is a DOAS (Differential Optical Absorption Spectroscopy) fitting technique that involves a multi-linear regression of GOME-measured optical densities against a number of reference spectra. It provides trace gas column amounts along the viewing path of the instrument (Burrows et al., 1999). The differential absorption of trace species along the absorption path is modelled according to Beer's law

$$\mathrm{d}I(\lambda) = -I(\lambda)\sigma(\lambda)C(s)\,\mathrm{d}s \qquad (1)$$

where the incremental change of intensity $dI(\lambda)$ at wavelength λ through a slant path distance ds is proportional to the absorption cross-section $\sigma(\lambda)$ times the intensity $I(\lambda)$ and the absorber column amount $C(s)$. When there are several weak absorbers, the contributions are additive, provided that the total optical density remains small and therefore saturation does not occur. The ozone retrieval was performed between 325 and 335 nm, while the NO_2 retrieval used a fitting window between 425 and 450 nm. Details about the spectral fitting can be found in Burrows et al. (1999) and Thomas et al. (1998).

The resulting trace gas slant columns are then converted to geometry-independent vertical column amounts through division by appropriate air mass factors (AMF). Air mass factors describe the enhancement of the absorption of a given trace gas due to slant paths of incident light in the atmosphere:

$$\mathrm{AMF} = \frac{\tau_{\mathrm{slant}}}{\tau_{\mathrm{vert}}} \tag{2}$$

where τ_{slant}, τ_{vert} are the slant and the vertical optical densities, respectively. The slant optical densities, i.e. the AMFs, are derived from radiative transfer calculations and do not require input from GOME measurements other than viewing geometry and geolocation information. However, AMFs depend further on the albedo of the underlying surface and the altitude of the reflecting surface, which can be either the ground or the cloud-top, and atmospheric profiles of temperature, pressure and trace gas concentration. Radiation propagation through clouds is not considered. Instead, clouds are treated as reflecting boundaries in the atmosphere.

Ozone AMFs were calculated on the basis of the TOMS V7 ozone profile climatology (Klenk et al., 1983; Chu et al., 1989) using LIDORT (Spurr et al., 2001), and are obtained from look-up tables by neural network techniques. The total ozone content is derived from an iterative procedure that searches for the best suited ozone profile, i.e. the AMF as function of the integrated profile content (and a number of other geophysical parameters, as mentioned above). A different approach is followed for nitrogen dioxide AMFs, which are calculated in two steps. A fast radiative transfer model calculates AMFs on-line, considering only single scattering effects. The multiple scattering is then accounted for by multiplicative correction factors that were derived from radiative transfer simulations (Rozanov et al., 1997), restored from a look-up table.

A common way of calculating the vertical column density (VCD) of a species (here nitrogen dioxide) is to calculate first a representative slant column $\mathrm{SC}_{\mathrm{total}}$ by adding the fitted slant column SC and a climatological slant column content below clouds (if present), followed by a division through the total air mass factor $\mathrm{AMF}_{\mathrm{total}}$ which is the weighted average of clear sky and cloudy AMFs. A so-called ghost vertical column (GVC) below clouds is derived from climatological trace gas profiles. The vertical column density now reads:

$$\mathrm{VCD} = \frac{\mathrm{SC}_{\mathrm{total}}}{\mathrm{AMF}_{\mathrm{total}}} = \frac{\mathrm{SC} + f_{\mathrm{c}} \times \mathrm{GVC} \times \mathrm{AMF}_{\mathrm{c}}}{f_{\mathrm{c}} \times \mathrm{AMF}_{\mathrm{c}} + (1 - f_{\mathrm{c}}) \times \mathrm{AMF}_{\mathrm{g}}} \tag{3}$$

where f_{c} is the cloud coverage between 0 and 1, SC the fitted slant column, GVC the ghost vertical column, and $\mathrm{AMF}_{\mathrm{g}}$ and $\mathrm{AMF}_{\mathrm{c}}$ the air mass factors down to ground and to cloud-top.

Recent studies (Lambert et al., 1999; 2000) comparing GOME and TOMS data against ground-based measurements indicate that the agreement of GOME total ozone columns is within 2–4% for solar zenith angles below 70°, which is the case in our study. Total nitrogen dioxide columns derived from GOME, other satellite instruments (HALOE, POAM) and ground-based measurements agree in general within 5–20%, but within $\pm 5 \times 10^{14}$ molecules cm^{-2} in areas of low NO_2 in the planetary boundary layer and within $\pm 8 \times 10^{14}$ molecules cm^{-2} in areas of very low slant columns of nitrogen dioxide. Recent studies (Richter and Burrows, 2002; Martin et al., 2002) showed that GOME nitrogen dioxide measurements partially suffer from instrumental artefacts that may cause a temporally varying offset in the slant columns up to 2×10^{15} molecules cm^{-2} depending on the time of the year. These structures, however, appear to be similar from year to year. For November 2001, a slight underestimation of retrieved NO_2 slant columns around 4×10^{14} molecules cm^{-2} can be estimated using the offset determined for 1998/1999 by Martin et al. (2002).

2.2. *The chemical transport model ROSE*

The spatial background distribution and the temporal evolution of stratospheric ozone and nitrogen dioxide are simulated using the 3D global chemical-transport model ROSE as described in detail in Rose and Brasseur (1989), Granier and Brasseur (1991) and Riese et al. (1999). The model covers the relevant gas-phase stratospheric chemical processes.

Heterogeneous processes on polar-stratospheric clouds and on sulfuric aerosols are also included in the model. It accounts for about 100 reactions, including oxygen, hydrogen, carbon, nitrogen, chlorine and bromine species. The chemical rate constants and cross-sections are taken from Sander et al. (2000). Photolysis rates are derived from a look-up table depending on solar zenith angle, ozone column and altitude. The chemical rate equations are solved by considering a chemical equilibrium state for the short-lived species (e.g. ClO, NO, HO, BrO). A semi-implicit scheme is used for the integration of the more stable reactants (e.g. HNO_3, N_2O, NH_4). All short-lived species are grouped and integrated using families, e.g. $ClO_x = Cl + ClO$, $NO_x = NO + NO_2$. All long-lived species are transported using the semi-Lagrangian scheme of Smolarkiewicz and Rasch (1991). Wind and temperature fields are derived from 24-h analyses of the UK Meteorological Office (UKMO) following Swinbank and O'Neill (1994), which are available for pressure levels from ground up to 0.3 hPa. This data set defines a consistent synoptic state using satellite-based temperature soundings and radiosonde observations assimilated in a global circulation model (GCM).

For this study we use a ROSE version with a 5.6° × 5° longitude–latitude spherical grid on 43 log-pressure levels between 0 and 60 km altitude, resulting in a vertical step size of 1.3 km. In the model's troposphere all chemical species are relaxed to 2D model data (Brasseur et al., 1995) with a timescale of 10 d.

This data set describes climatological zonal mean distributions of a sub-set of species relevant for stratospheric conditions. The model's tropopause is defined by a potential vorticity of 1.6 pvu (see section 3.2) or a potential temperature of 380 K for the tropics. In order to investigate the impact of the tropopause height model runs were also performed for a different tropopause height corresponding to 3 pvu (see section 3.4). The model runs covering the period 6–14 November 2001 were initialised with data from the DFD near-real-time (NRT) service (http://auc.dfd.dlr.de/ROSE). This NRT service delivers vertical ozone profiles using GOME total ozone column densities that are assimilated into ROSE on an operational basis.

3. Results

3.1. Synoptic analysis

The meteorological situation during the weather event is characterised by strong surface winds and heavy rainfall. Figure 1 (left panel) shows an intense upper level trough that pushes far to the Southwest of Europe and meets the Algerian coast from west on 9 November 2001. The UKMO analysis of the temperature and the geopotential height is given at the 464 hPa level (∼6 km). The METEOSAT-7 IR-image from the same day (Fig. 2, left panel) shows that the cloud systems of the frontal zone extend from Finland across Central Europe to Spain. The cold front made the surface temperatures in Andalusia (Spain) drop at midday

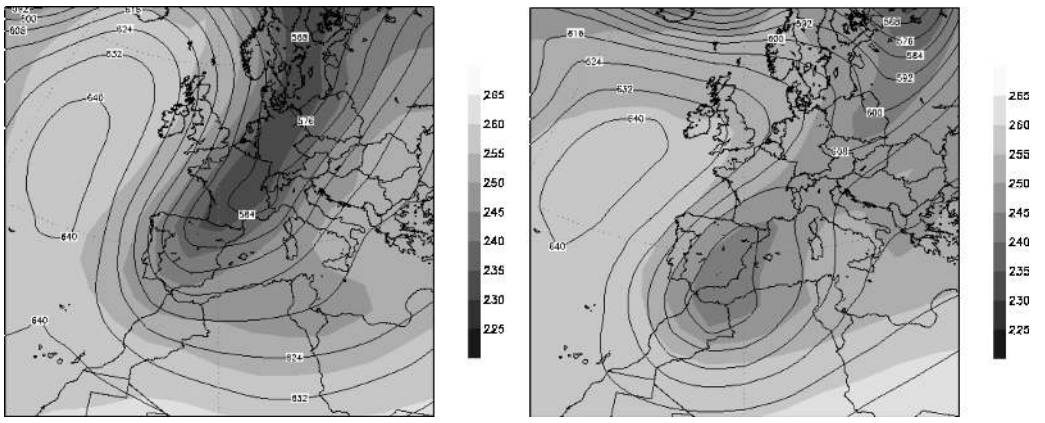

Fig. 1. UKMO analysis of the temperature in K (greyscale) and the geopotential height in gpm (isolines) at 464 hPa (∼6 km) at 12:00 UTC for 9 November 2001 (left panel) and 10 November 2001 (right panel).

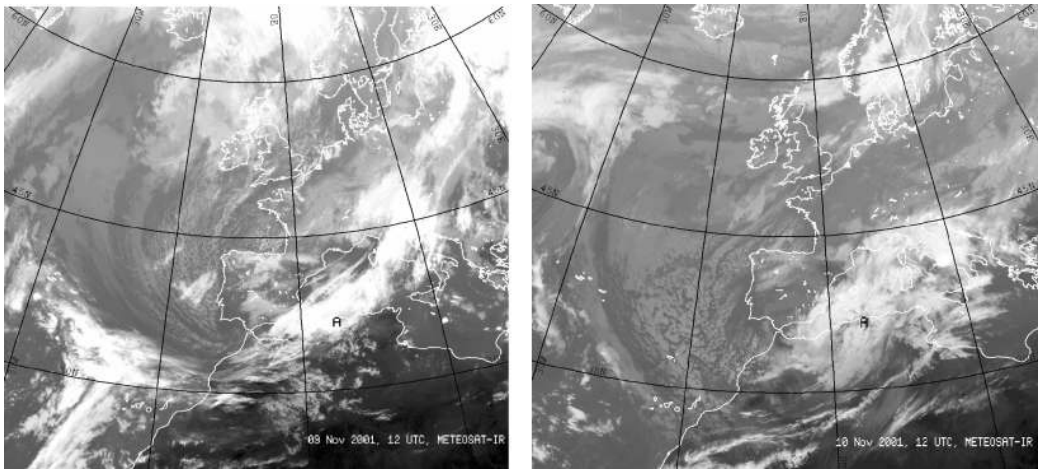

Fig. 2. METEOSAT-7 IR data at 12:00 UTC for 9 November 2001 (left panel) and 10 November 2001 (right panel); A, Algiers.

from 25 to 18 °C and to frost at night. Heavy rainfall begins at the Algerian coast on late 9 November 2001 and ends at about noon on 10 November 2001. Cyclonic curvature and shear vorticity define the positive vorticity advection (PVA) at the Algerian coast. This PVA implies a deepening of the low-pressure system and a cut-off low developed with maximum potential vorticity in that area (Fig. 1, right panel). On its east side very warm lower air from the tropics was mixed with higher cold air of arctic origin, leading to a highly unstable air mass and initiating a cyclogenesis with a tropical warm core which is unusual at these latitudes. Two processes intensified the convective development: (1) the cold maritime arctic air crosses over the still warm Mediterranean, where it picks up moisture and meets maritime subtropical air and (2) the strong surface winds from north-west towards the mountainous African coast caused intense orographic rainfall. Figure 2 shows the clouds rotating around Algiers due to the cut-off low process. On both days, 9 and 10November 2001, extraordinary rainfall rates of 126 L m^{-2} in 12 h and 136 L m^{-2} in 6 h were reported which led to the flooding disaster in Algeria. The regional maximum rain rate in 6 h in Algeria was more than the 30 years monthly mean November rainfall rate of 129 L m^{-2}.

3.2. *Ozone and PV analysis*

The total ozone distribution as derived from GOME backscatter measurements between 9 and 11 November 2001 is shown in Fig. 3, left panels. The GOME overpass time over the area is around 10:20 h local time (here close to 10:20 UTC) on each day due to the sun-synchronous polar orbit of ERS-2. High gradients in total ozone column from pixel to pixel (several 10 DU) indicate strong dynamic activity over Europe. As early as in 1950 Reed showed that the total ozone column is an excellent tracer for upper level weather systems modulated by tropopause and lower stratosphere variability. A well suited synoptic diagnosis quantity is the corresponding isentropic PV at 330 K (Hoskins et al., 1985) which is depicted for each day on the right panels of Fig. 3. PV is a conservative quantity in frictionless and adiabatic flow and the values on the 330 K isentrope correlate well with the total ozone column at midlatitudes (Hood et al., 1999). The essential physics of the relationship between total ozone and vorticity is described in Vaughan and Price (1991).

At the beginning of the investigated period, we observe low ozone levels below 200 DU over Northern Europe on 9 and 10 November 2001 forming an ozone mini-hole (Figs. 3a and c). It is accompanied by a high-pressure system which is characterised by an elevated tropopause and a negative PV anomaly and governs the large-scale motion field (Fig. 3b). Hence, on its front side (east) an upper level trough is forming over Scandinavia and the Baltic. It moves eastwards and rapidly expands in a south-westward direction leading to enhanced ozone levels over Spain (Fig. 3c). While the upper-level trough deepens, the tongue of high PV elongates and thins with a pronounced NE–SW axis (Fig. 3d). The formation is due to equatorward

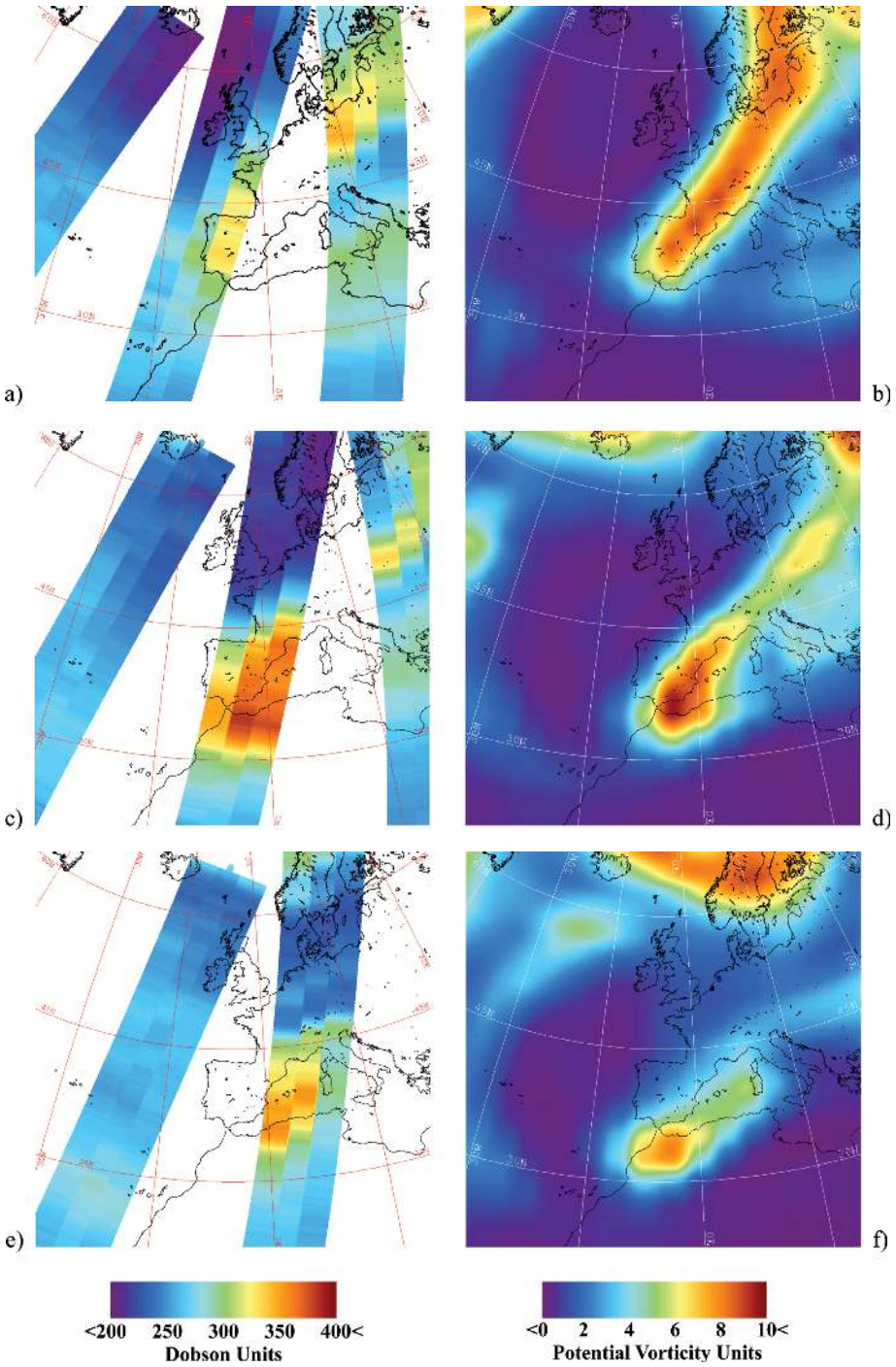

Fig. 3. GOME-measured ozone distribution on 9 November 2001 (a), 10 November 2001 (c), 11 November 2001 (e) and corresponding isentropic potential vorticity on the 330 K surface derived from UK Meteorological Office stratospheric analyses for the same days at 12:00 UTC (b, d, f).

Rossby wave breaking (McIntyre and Palmer, 1985). From 10 to 11 November 2001, the structure formed by high PV levels breaks up and the tip of the tongue separates, rolling up cyclonically, forming a cut-off low centred over Morocco (Fig. 3f). The core shows high PV values of about 9.3 pvu (1 pvu = 10^{-6} K m^2 kg^{-1} s^{-2}), indicating a reservoir of polar stratospheric air masses at a very pronounced southern location of 35°N. Associated with the equatorward Rossby wave breaking event we observe high total ozone column values over Southern Spain, Morocco, Algeria and the Mediterranean Sea (Figs. 3c and e). The total ozone content at these low latitudes increases by about 100 DU, from 280 DU on 8 November 2001 to 380 DU on 10 November 2001. On 11 November 2001 the maximum total ozone has decreased again to 355 DU.

In order to investigate the equatorward location of the PV maximum from a climatological and statistical point of view, 11 years of UKMO analysis data were examined. Potential vorticity was determined on a daily basis from 1992 to 2002 at 35°N and for all longitudes on the 330 K isentrope. During this period PV values reached a similar level only on four days, which underlines the strong meridional transport during this outstanding weather event.

Besides horizontal transport phenomena we also examined changes in the vertical structure of the atmosphere. The dynamic tropopause can be defined as an isosurface of potential vorticity. Hoerling et al. (1991) discussed different threshold values from 1 to 3.5 pvu for the definition of the dynamic tropopause while the WMO recommended the 1.6 pvu isoline at midlatitudes (WMO, 1985). According to Price and Vaughan (1993), this is reasonable when studying cut-off lows, as it is the case here. However, outside the cut-off low the 3 pvu isoline may be a more representative value. In our case study the 3 pvu isoline is about 100 hPa higher than the 1.6 pvu isoline in the area with the cut-off low, while the effect is less pronounced outside where changes are below 25 hPa. The impact of different tropopause heights is discussed in more details in sections 3.4 and 3.5. The tropopause lowering within the upper level trough leads to an increase of the stratospheric air reservoir and contributes to an increase of the total ozone column amounts. By means of the PV as a stratospheric tracer, the folding shows isentropic flow to its western flank, indicating stratospheric intrusion. As depicted in Fig. 3d the tip of the equatorward pointing PV structure broke away on 10 November 2001, forming a cut-off low. For that day, Fig. 4 (left panel) shows a north–south cross-section of PV and potential temperature along the Greenwich meridian from 20° to 60°N, based on analyses of the European Centre of Medium Range Weather Forecast (ECMWF).

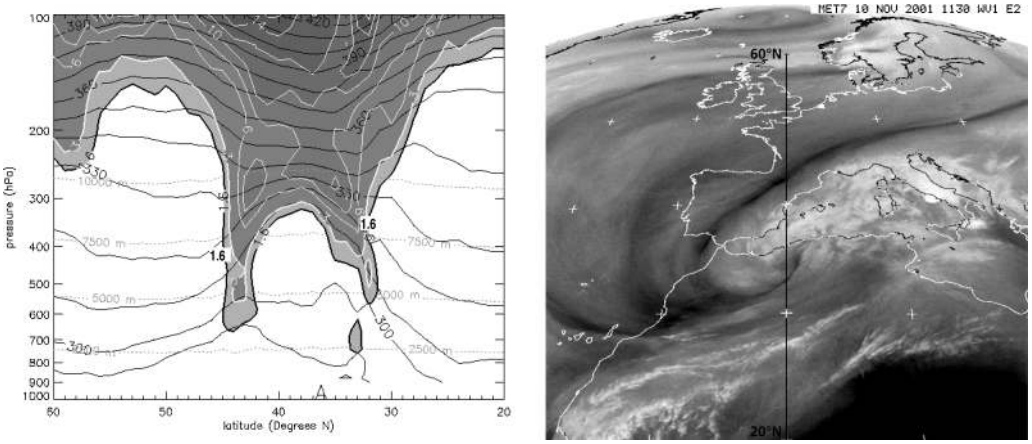

Fig. 4. PV north–south cross-sections for 10 November 2001 at 0°W (left panel) along the Greenwich meridian and METEOSAT-7 water vapour image (right panel) of 10 November 2001 11:30 UTC. Potential vorticity isocontours are in white while isentropes are in black. The 1.6 pvu isoline (thick black line, left panel) denotes the dynamical tropopause. The next isoline (white) corresponds to 3 pvu and the difference to 1.6 pvu is shaded in bright grey. The geographical position of Algiers is marked by the A at 36°N in the left panel. The Greenwich meridian at 0°W is marked by the black line in the METEOSAT-7 image (Source: UK Met Office).

The cyclogenesis around Algiers (36°N) is associated with a significant enfolding of the tropopause where stratospheric ozone-rich air intrudes to 700 hPa on 10 November 2001 and splits up into two tongues in the cross-section (Fig. 4, left panel). This is due to the cyclonic spin of the fold around the forming cut-off low, which is confirmed by the METEOSAT-7 water vapour image from 10 November 2001 at 11:30 UTC (Fig. 4, right panel). The dry intrusion of stratospheric air into the cyclone is apparent: it forms a streamer indicated by a dark narrow band reaching straight from Russia to Morocco and then spinning cyclonically.

3.3. Nitrogen dioxide observations

The NO_2 distribution derived from GOME measurements does not show a similar temporal and spatial pattern as ozone and PV in the same period. However, on 10 November 2001, enhanced NO_2 levels are observed along the Cantabric coast (Spain) and over Morocco (also over Macedonia), which coincides with night-time lightning activity (Fig. 5, upper panels). Enhanced NO_2 concentrations in the upper troposphere caused by lightning activity have recently been measured by Huntrieser et al. (2002); these plumes may persist for several hours. Another area with higher nitrogen dioxide levels is visible over France which can be attributed to tropospheric pollution. Here, GOME cloud coverage results indicate a low cloudiness of below 20% providing satellite measurements down to surface levels. On 11 November 2001, during and after heavy thunderstorms, an NO_2 plume is observed over the western Mediterranean Sea around the Balearic Islands and towards the North-African coast (Fig. 5, lower left).

Before the cold front reached the area on 8 November 2001 the typical NO_2 vertical column was around $(2.5–3.5) \times 10^{15} \pm 3.5 \times 10^{14}$ molecules cm^{-2}, but higher over France, while an unusually high maximum total content of $7.27 \times 10^{15} \pm 4.4 \times 10^{14}$ molecules cm^{-2} was observed on 11 November 2001. A negative bias of about -1.4×10^{14} molecules cm^{-2} need to be considered to correct for possible artefacts in GOME backscatter data (Martin et al., 2002). The given error levels are derived from the slant column fitting precision (i.e. standard deviation), the corresponding cloud fitting precision and an assumed precision of AMFs of 1% which is due to radiative transfer modelling. Errors of reference spectra were not considered. The origin of the NO_2 plume is further analysed in section 3.5.

3.4. ROSE simulations of nitrogen dioxide

ROSE simulations starting on 6 November 2001 were performed to compare simulated stratospheric nitrogen dioxide distributions with coincident GOME observations during the period of interest. The models tropopause is defined as described in section 2.2 using the 1.6 pvu or the 380 K potential temperature isoline. The differences between GOME NO_2 total column results and modelled stratospheric results can then be used to estimate the tropospheric NO_2 content which is further discussed in section 3.5.

To separate the effect of transport from local chemical transformations we analysed the temporal development of total ozone and a tracer (chemically passive ozone, initialised with ozone values from 5 November 2001) for a fixed model location at 0°E, 40°N. Air masses with high ozone loading were transported southward, as confirmed by PV analysis (see section 3.1). We observe a maximum increase of the simulated total ozone column during 8 to 10 November 2001 and these results compare qualitatively well with coincident GOME observations. By comparing the temporal behaviour of ozone with that of the tracer we estimate that chemical transformations locally only contribute 5% to the simulated change of the stratospheric ozone column.

Recent comparisons of ROSE results with observations showed that the NO_2 temporal behaviour is reasonably well described by the model (Sen et al., 1998; Toon, 1991). Maximum daily NO_2 columns are simulated after sunset (at surface levels) before NO_2 is converted mainly into its night-time reservoir N_2O_5. Minimum NO_2 columns are present after sunrise when most of the NO_2 is quickly photolyzed into NO, thus lowering the total content by one order of magnitude. Stratospheric total NO_2 levels slightly recover during day time, typically by about 1×10^{14} molecules cm^{-2} h^{-1}. To evaluate the model performance we compare the simulated minimum NO_2 values with available HALOE November observations in the midlatitudes (Gordley et al., 1996) for sunrise conditions (http://haloedata.larc.nasa.gov/Haloe/home.html). A direct comparison of the spatial NO_2 distributions with independent space-borne measurements is compromised due to missing data during the period of interest. ROSE NO_2 minimum total column values above 20 km altitude compare well with HALOE measurements with model values being slightly higher. Model results are in excellent agreement with HALOE observations near the stratospheric

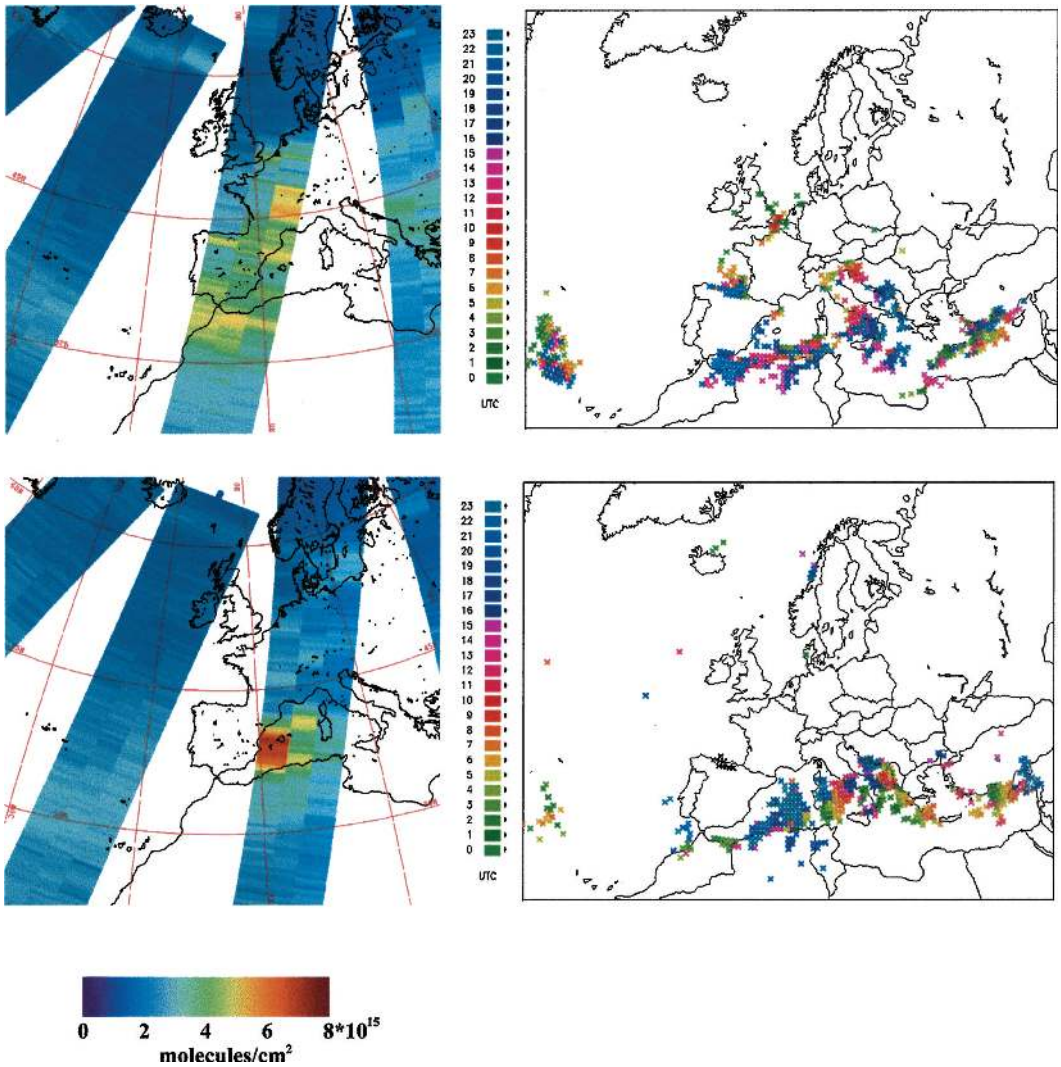

Fig. 5. GOME-measured nitrogen dioxide distribution on 10 November 2001 (upper left) and 11 November 2001 (lower left), and lightning statistics for both one day earlier, the 9 November 2001 (upper right) and 10 November 2001 (lower right). Slightly increased column densities are observed over the strait of Gibraltar and along the Cantabric coast on 10 November 2001 (upper left), where both night-time lightning activity was reported. On 11 November 2001, unusually high NO_2 column densities of about 7.2×10^{15} molecules cm^{-2} were measured over the Mediterranean Sea (lower left). Lightning statistics were taken from http://www.wetterzentrale.de.

NO_2 maximum around 30 km altitude. Modelled NO_2 columns near the 100 hPa level ($\sim$16 km) tend to be higher than corresponding HALOE values, but deviations stay within the known bias of HALOE. The simulated average zonal variability of 10% for the NO_2 column corresponds well with HALOE observations.

At the GOME overpass time during the period of interest the temporal changes of NO_2 due to chemical transformation are typically low. ROSE stratospheric NO_2 columns calculated at 10:00 UTC decrease smoothly from 2.1×10^{15} molecules cm^{-2} on 6 November 2001 to 1.6×10^{15} molecules cm^{-2} on 11 November 2001 at 40°N 0°E, where GOME-derived

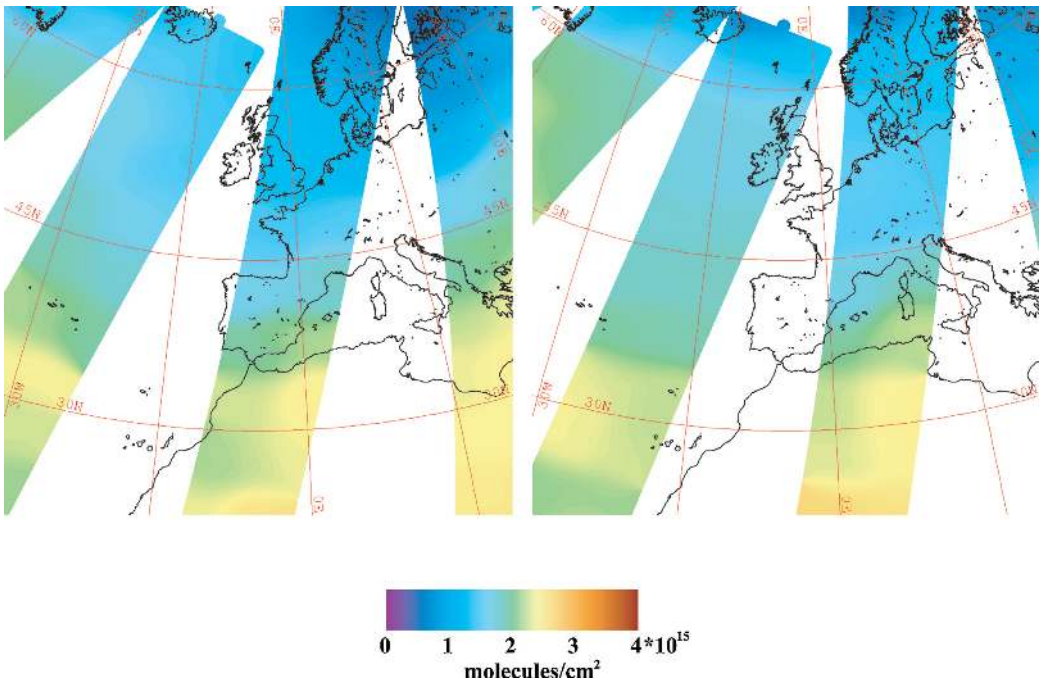

Fig. 6. Total stratospheric nitrogen dioxide content for 10 November 2001 (left panel) and 11 November 2001 (right panel) as calculated by ROSE at GOME local overpass times (10:20 LT). The maximum stratospheric content is about 2.6×10^{15} molecules cm^{-2} over the Saharan desert, while it is around 1.8×10^{15} molecules cm^{-2}in the area southward of the Balearic Islands where measured NO_2 values were highest. The day-to-day variation in the latter area remains small.

NO_2 levels were highest. Therefore, the temporal resolution of UKMO analysis data of about 24 h is sufficiently high to describe the impact of stratospheric transport. The variation from 10 to 12 November 2001 is lower than 5×10^{14} molecules cm^{-2}. ROSE NO_2 column results at GOME overpass time (10:20 LT) on 10 and 11 November 2001 are shown in Fig. 6.

The ROSE-modelled spatial distribution of NO_2 is dominated by the bulk of NO_2 in the stratosphere around 30 km. The relatively low NO_2 columns over Northern and Central Europe and even down to Spain on 10 November 2001 can be attributed to wave-like transport in stratospheric levels at higher latitudes. Measured ozone fields and PV analysis indicate a more pronounced meridional transport in lower atmospheric levels especially on 9 November 2001 (Figs. 3a and b). The simulated NO_2 column content during the GOME overpass time varies between $(0.9–2.6) \times 10^{15}$ molecules cm^{-2} from North to South, which is lower than corresponding GOME measurements outside the NO_2 plume over water surfaces and high latitudes. The strong increase of measured NO_2 levels on 11 November 2001 (see Fig. 5, lower left) does not appear in the simulations. Note, however, that ROSE does not consider tropospheric emissions (section 2.2). The tropospheric NO_2 content is further discussed in the following section.

3.5. *Derivation and analysis of tropospheric nitrogen dioxide*

Several methods to derive the nitrogen dioxide content in the troposphere are discussed in the literature. Velders et al. (2001) apply both the so-called tropospheric excess method (Richter and Burrows 2002) and image processing technique to derive the tropospheric NO_2 columnar content. The tropospheric excess method allows one to separate tropospheric and stratospheric contributions to the total NO_2 content under the assumption of a relatively stable (both in time and space) NO_2 distribution over the free Pacific Ocean. Lauer et al. (2002) compare tropospheric NO_2 columns derived from GOME measurements and results of a coupled chemistry–climate model. The

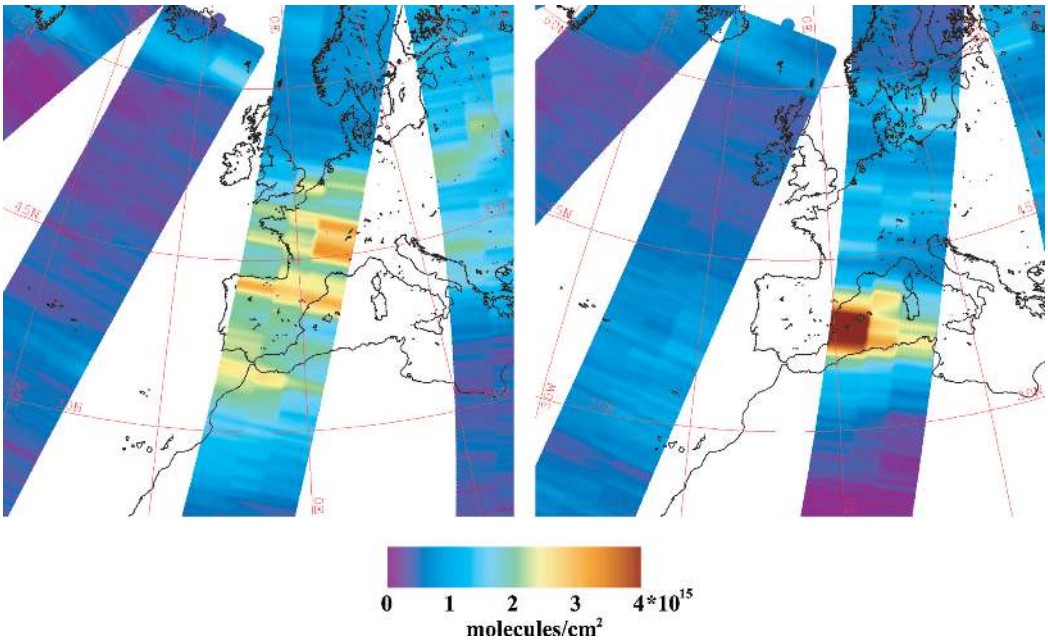

Fig. 7. Tropospheric nitrogen dioxide columns derived by subtracting ROSE results from GOME measurements for 10 November 2001 (left panel) and 11 November 2001 (right panel). Maximum values on 11 November 2001 are around 5.5×10^{15} molecules cm^{-2}.

tropospheric NO_2 columns were again derived using the tropospheric excess method. In both studies mean values (monthly or for a number of consecutive days) of the tropospheric NO_2 content are derived. Martin et al. (2002) apply a chemical transport model and take into account the variability of NO_2 AMFs as a function of the NO_2 profile shape, of the surface reflectivity and under the presence of clouds. Again, tropospheric nitrogen dioxide levels are derived on a monthly basis.

In our study we derive the NO_2 tropospheric content with the temporal and spatial resolution of GOME/ERS-2 orbits. Since we use ROSE model data only above the tropopause level (see section 2.2) we can derive the tropospheric column amount of NO_2 by subtracting the stratospheric component from the GOME NO_2 total column measurements. By combining model results and GOME observations on 10 and 11 November 2001 we get the tropospheric column content at GOME observation time. In undisturbed areas and over the free ocean tropospheric column values are in general around 1×10^{15} molecules cm^{-2} and below while higher tropospheric columns of about (2–3) $\times 10^{15}$ molecules cm^{-2} are present over France, Northern Spain, and the Street of Gibraltar on 10 November 2001 (Fig. 7, left side). We calculate a maximum tropospheric NO_2 column content of about $5.5 \times 10^{15} \pm 6.3 \times 10^{14}$ molecules cm^{-2} over the Western Mediterranean (Fig. 7, right side).

The error is calculated from the standard deviation of the GOME NO_2 result (section 3.3) and the corresponding uncertainty of the ROSE NO_2 results of about 10%. A possible negative bias due to instrumental features (section 2.1) is not included in the calculated maximum content and its error budget. The absolute value of the bias remains well below 10% of the maximum NO_2 value but becomes more important over areas with lower total content. A change of the models tropopause level from 1.6 to 3 pvu does not have a significant impact on calculated tropospheric NO_2 columns. The simulations reveal a mean difference of about $\pm 2 \times 10^{13}$ molecules cm^{-2} and an increase of tropospheric levels around 1×10^{13} molecules cm^{-2} in the area with highest NO_2 values which is well below the uncertainty of the calculated tropospheric NO_2 column.

The origin of the derived NO_2 plume on 11 November 2001 is further analysed. We first notice that there is a delay of one day between the ozone maximum content and the nitrogen dioxide maximum. We further know that the stratospheric NO_2

abundance in high latitudes is low during the winter season. It is therefore unlikely that the observed enhanced NO_2 levels are due to advection of NO_2 rich air masses above the troposphere from high latitudes. The cloud coverage was high (>90%) over the area with the NO_2 plume on 11 November 2001 and satellite observations of the PBL were compromised. Under these circumstances, the GOME-derived total nitrogen dioxide content is dominated by the NO_2 content above the clouds [see also eq. (3)] and also the contribution of the climatological ghost column (below clouds) to the total content is well below 5% and may not contribute significantly to total NO_2 levels. We therefore conclude that enhanced NO_2 levels on 11 November 2001 are due to local processes in the troposphere above clouds, e.g. lightning activity during the night from 10 to 11 November 2001 (Fig. 5, upper right), and polluted air masses uplifted from the planetary boundary layer by the thunderstorms, as also described in Huntrieser et al. (2002). To our knowledge other natural tropospheric sources of NO_2 over water surfaces are unknown. However, air masses from the PBL may not necessarily originate from the same area but can be due to advection of polluted air masses over France and Spain in the troposphere, as indicated by enhanced GOME-measured NO_2 levels on 10 November 2001 (Fig. 5, upper left). The transport processes are endorsed by a 3D backward trajectory analysis using the FLEXTRA model (Stohl et al., 1999) based on ECMWF analyses data. The simulation started in the NO_2 plume at the GOME overpass time (1020 UTC) and ran backwards for 60 h. The results show advection and uplifting of tropospheric air masses up to 4–7 km from regions where NO_2 levels were high (Central and Southern France, Italian Po valley). Other trajectories follow the thunderstorm movement in the cut-off low during the night from 10 to 11 November 2001. Strong lightning activity was reported during this night in a triangle between Corsica, the Balearic Islands and the North African coast (Fig. 5, lower right), hence supporting the origin of nitrogen dioxide from lightning. The trajectory analysis gave evidence that air masses were finally transported with easterly winds following the cyclonic movement to the area where NO_2 levels were highest.

The analysis reveals further that air masses were moved up from the PBL to 4–7 km, even up to 10 km above sea level by about 10 h before the GOME overpass. Other trajectories indicate air masses that were lifted up 36 h earlier but then moving in the same height range (4–7 km) with the thunderstorms.

4. Summary and conclusions

We used satellite-based trace gas measurements, synoptic data, potential vorticity analysis and results from a chemical transport model to describe the temporal and spatial evolution of the Algiers cold front from 9 to 11 November 2001. Our results are summarised as follows:

The dynamically induced transport of cold air from arctic latitudes down to subtropical latitudes over the warm Mediterranean Sea within 24 h led to severe thunderstorms and extraordinarily high rainfall rates at these latitudes. The formation of a cut-off low could be traced and we observed a tropopause lowering below 3 km indicating a pronounced intrusion of stratospheric air masses to tropospheric levels. High potential vorticity values of about 9.3 pvu on the 330 K isentrope at the remarkably low latitude of 35°N emphasise the strong meridional transport.

Concerning the trace gas distributions we could show that the enhancements of the total ozone and nitrogen dioxide columns over the western Mediterranean Sea were of different nature. The increase of ozone levels originates from the large-scale meridional transport of air masses with high ozone content to subtropical regions in the lower stratosphere, which is confirmed by PV analysis but also ROSE simulations. Comparison of GOME results and ROSE simulations showed that the observed enhancement of NO_2 is confined to the troposphere. The combination of results of the stratospheric chemistry model and GOME observations allow to quantify tropospheric NO_2 levels at the temporal and spatial resolution of GOME orbits. A maximum tropospheric content of about 5.5×10^{15} molecules cm^{-2} was derived which is attributed to lightning activity and advected NO_2-enriched air masses from the PBL. Our method avoids the limitations of the tropospheric excess method and can be applied on a global scale in a near-real-time environment. It is therefore possible to provide quickly information about enhanced tropospheric nitrogen dioxide levels, as they occur frequently over industrialised areas but also during biomass burning events. The method is not confined to a certain satellite instrument but sensor-specific features such as the known diffuser plate structures in GOME backscatter data need to be taken into account. Further refinement and validation will help to apply it successfully to data from spaceborne sensors with higher spatial resolution, e.g. from the Scanning Imaging Absorption Spectrometer for Atmospheric Cartography (SCIAMACHY) on board

ENVISAT as well as to data from future satellite missions, among them GOME-2 on board METOP (to be launched in 2005).

5. Acknowledgments

We are grateful to our reviewers that helped us with their remarks to strengthen the paper. Our colleagues from the European Centre for Medium Range Weather Forecast, and the UK Meteorological Office kindly provided much appreciated synoptic data. We thank our DLR colleagues D. Loyola, T. Ruppert and S. Giegerich for help with the GOME data processing, image generation and preparation of this manuscript. We are grateful to G. Brasseur for providing the ROSE CTM.

REFERENCES

Bluestein, H. 1993. Synoptic–dynamic meteorology in midlatitudes, volume II. Observations and theory of weather systems. Oxford University Press, Oxford, 594 pp.

Brasseur, G., Hitchman, M. H., Walters, S., Dymek, M., Falise, E. and Pirre, M. 1995. An interactive chemical dynamical radiative two-dimensional model of the middle atmosphere. *J. Geophys. Res*. **95**, 5639–5655.

Brunner, D., Staehelin, J., Jeker, D., Wernli, H. and Schumann, U. 2001. Nitrogen oxides and ozone in the tropopause region of the Northern Hemisphere: Measurements from commercial aircraft in 1995/1996 and 1997. *J. Geophys. Res.* **106,** 27673–27699.

Burrows, J. P., Weber, M., Buchwitz, M., Rozanov, V., Ladstätter-Weißenmayer, A., Richter, A., de Beek, R., Hoogen, R., Bramstedt, K., Eichmann, K.-U., Eisinger, M. and Perner, D. 1999. The Global Ozone Monitoring Experiment (GOME): Mission concept and first scientific results. *J. Atm. Sci.* **56**, 151–175.

Chu, W. P., McCormick, M. P., Lenoble, J., Brogniez, C. and Pruvost, P. 1989. SAGE II Inversion Algorithm. *J. Geophys. Res.* **94**, 8339–8351.

Gordley, L. L., Russel III, J. M., Mickley, L. J., Frederick, J. E., Park, J. H., Stone, K. A., Beaver, G. M., McInerney, J. M., Deaver, L. E., Toon, G. C., Murcray, F. J., Blatherwick, R. D., Gunson, M. R., Abbatt, J. P. D., Mauldin III, R. L., Mount, G. H., Sen, B. and Blavier, J.-F. 1996. Validation of nitric oxide and nitrogen dioxide measurements made by the Halogen Occultation Experiment for UARS platform. *J. Geophys. Res.* **101**, D6, 10 241–10 266.

Granier, C. and Brasseur, G. 1991. Ozone and other trace gases in the Arctic and Antarctic regions: Three-dimensional model simulations. *J. Geophys. Res.* **96**, 2995–3011.

Hoerling, M. P., Schaack, T. K. and Lenzen, A. J. 1991. Global objective tropopause analysis. *Mon. Weather Rev.* **119**, 1816–1831.

Hood, L., Rossi, S. and Beulen, M. 1999. Trends in lower stratospheric zonal winds, Rossby wave breaking behavior, and column ozone at northern midlatitudes. *J. Geophys. Res*, **104**, 24 321–24 339.

Hoskins, B. J., McIntyre, M. E. and Robertson, A. W. 1985. On the use and significance of isentropic potential vorticity maps. *Q. J. R. Meteorol. Soc.* **111**, 877–946.

Huntrieser, H., Feigl, Ch., Schlager, H., Schröder, F., Gerbig, Ch., van Velthofen, P., Flatøy, F., Théry, C., Petzold, A., H. and Schumann, U. 2002. Airborne measurements of NO_x, trace species and small particles during the European Lightning Nitrogen Oxides Experiment. *J. Geophys. Res.* **107**, 10.1029/2000JD000209, ACH 5-1–ACH 5-24.

Kentarchos, A. S., Davies, T. D. and Zerefos, C. S. 1998. A low latitudinal stratospheric intrusion associated with a cut-off low. *Geophys. Res. Lett*. **25**, 67–70.

Koelemeijer, R. B. A. and Stammes, P. 1999. Validation of Global Ozone Monitoring Experiment cloud fractions for accurate ozone column retrieval. *J. Geophys. Res.* **104**, 18 801–18 814.

Klenk, K. F., Bhartia, P. K., Hilsenrath, E. and Fleig, A. J. 1983. Standard ozone profiles from balloon and satellite data sets. *J. Climate Appl. Meteorol.* **22**, 2012–2022.

Kuze, A. and Chance, K. V. 1994. Analysis of cloud-top height and cloud coverage from satellites using the O_2 A and B bands. *J. Geophys. Res.* **99**, 14 481–14 491.

Lambert, J.-C., Van Roozendael, M., De Maziere, M., Simon, P. C., Pommereau, J.-P., Goutail, F., Sarkissian, A. and Gleason, J. F. 1999. Investigation of pole-to-pole performances of spaceborne atmospheric chemistry sensors with the NDSC. *J. Atmos. Sci.* **56**, 176–193.

Lambert, J.-C., Van Roozendael, M., Simon, P. C., Pommereau, J.-P., Goutail, F., Gleason, J. F., Andersen, S. B., Arlander, D. W., Bui Van, N. A., Claude, H., de La Noe, J., De Maziere, M., Dorokhov, V., Eriksen, P., Green, A., Karlsen Tornkvist, K., Kastad Hoiskar, B. A., Kyrö, E., Leveau, J., Merienne, M.-F., Milinevsky, G., Roscoe, H. K., Sarkissian, A., Shanklin, J. D., Staehelin, J., Wahlstrom Tellefsen, C. and Vaughan, G. 2000. Combined characterisation of GOME total ozone measurements from space using ground-based observations from the NDSC. *Adv. Space Res.* **26**, 1931–1940.

Lauer, A., Dameris, M., Richter, A. and Burrows, J. P. 2002. Tropospheric NO_2 columns: a comparison between model and retrieved data from GOME measurements. *Atmos. Chem. Phys.* **2**, 67–78.

Loyola D., Aberle B., Balzer W., Kretschel K., Mikusch E., MühleH., Ruppert T., Schmid C., Slijkhuis S., Spurr R., Thomas W., Wieland T. and Wolfmüller M. 1997. Ground segment for ERS-2 GOME data processor. *Proceedings of the 3rd Symposium on Space at the Service of our Environment*, Florence, Italy, ESA SP-414, 591–597.

Martin, R. V., Chance, K., Jacob, D. J., Kurosu, T. P., Spurr, R. J. D., Bucsela, E., Gleason, J. F., Palmer, P. I., Bey, I., Fiore, A. M., Li, Q., Yantosca, R. M. and Koelemeijer,

R. B. A. 2002. An improved retrieval of tropospheric nitrogen dioxide from GOME. *J. Geophys. Res.* **107**, 10.1029/2001JD001027, ACH 9-1–ACH 9-21.

McIntyre, M. E. and Palmer,T. N. 1985. A note on the general concept of wave breaking for Rossby and gravity waves. *PAGEOPH*. **123**, 964–975.

Price, J. D. and Vaughan, G. 1993. The potential for stratosphere-troposphere exchange in cut-off-low systems. *Q. J. R. Meteorol. Soc.* **119**, 343–365.

Reed, R. J. 1950. The role of vertical motions in ozone weather relationships. *J. Meteorol.* **7**, 263–267.

Richter, A. and Burrows, J. P. Tropospheric NO_2 from GOME measurements, 2002. *Adv. Space Res.* in press.

Riese, M., Tie, X., Brasseur, G. and Offermann, D. 1999. Three-dimensional simulation of stratospheric trace gas distributions measured by CRISTA. *J. Geophys. Res*, **104**, 16 419–16 435.

Rose, K. and Brasseur, G. 1989. A three-dimensional model of chemically active trace species in the middle atmosphere during disturbed winter conditions. *J. Geophys. Res.* **94**, 16 387–16 403.

Rozanov, V., Diebel, D., Spurr, R. J. D. and Burrows, J. P. 1997. GOMETRAN: Radiative transfer model for the satellite project GOME, the plane-parallel version. *J. Geophys. Res.* **102**, 16 683–16 695.

Sander, S. P., Ravishankara, A. R., Friedl, R. R., DeMore, W. B., Golden, D. M., Kolb, C. E., Kurylo, M. J., Molina, M. J., Hampson, R. F., Huie, R. E. and Moortgat, G. K. 2000. Chemical kinetics and photochemical data for use in stratospheric modeling. Eval. **13,** *JPL Publ.*, 00–3.

Sen B., Toon, G. C., Osterman, G. B., Blavier, J.-F., Margitan, J. J. and Salawitch, R. J. 1998. Measurements of reactive nitrogen in the stratosphere. *J. Geophys. Res.* **103**, 3571–3585.

Schumann, U. 1994. On the effect of emissions from aircraft engines on the state of the atmosphere. *Ann. Geophys*. **12**, 365–384.

Smolarkiewicz, P. K. and Rasch, P. J. 1991. Monotone advection on the sphere, An Eulerian versus semi-Lagrangian approach. *J. Atmos. Sci.* **48**, 793–810.

Spurr, R. J. D., Kurosu, T. P. and Chance, K. V. 2001. A linearized discrete ordinate radiative transfer model for atmospheric remote sensing retrieval. *J. Quantum. Spectros. Radiat. Trans.* **68**, 689–735.

Stohl, A., Haimberger, L., Scheele, M. P. and Wernli, H. 1999. An intercomparison of results from three trajectory models. *Meteorol. Appl.* **8**, 127–135.

Swinbank, R. and O'Neill, A. 1994. A stratosphere–troposphere data assimilation system. *Mon. Weather Rev.* **122**, 686–702.

Thomas, W., Hegels, E., Slijkhuis, S., Spurr, R. and Chance, K. 1998. Detection of biomass burning combustion products to Southeast Asia from backscatter data taken by the GOME spectrometer. *Geophys. Res. Lett*. **25**, 1317–1320.

Toon, G. C. 1991. The JPL MKIV interferometer. *Opt. Photonics News*, **2**, 19–21.

Vaughan, G. and Price, J. D. 1991. On the relation between total ozone and meteorology. *Q. J. R. Meteorol. Soc.* **117**, 1281–1298.

Velders, G. J. M., Granier, C., Portmann, R. W., Pfeilsticker, K., Wenig, M., Wagner, T., Platt, U., Richter, A. and Burrows, J. P. 2001. Global tropospheric NO2 column distributions: Comparing three-dimensional model calculations with GOME measurements. *J. Geophys. Res.* **106**, 12 643–12 660.

World Meteorological Organization (WMO). 1985. Atmospheric ozone 1985. *Global ozone research and monitoring report*, **16**, WMO, Geneva, Switzerland.